AFGL-TR-78-0130

LEVEL II

Problems in Modeling the Earth's Trapped Radiation Environment

JAMES I. VETTE
KING W. CHAN
MICHAEL J. TEAGUE

NATIONAL SPACE SCIENCE DATA CENTER
NASA GODDARD
GREENBELT, MD 20771

Scientific Report No. 1

1 October 1977 - 30 September 1978

AIR FORCE GEOPHYSICS LABORATORY
AIR FORCE SYSTEMS COMMAND
UNITED STATES AIR FORCE
HANSCOM AFB, MASSACHUSETTS 01731

(9) Scientific rept. no. 1, 1 Oct 77-30 Sep 78;

Unclassified

SECURITY CLASSIFICATION OF THIS PAGE (When Data Entered)

REPORT DOCUMENTATION PAGE	READ INSTRUCTIONS BEFORE COMPLETING FORM
(14) 1. REPORT NUMBER: AFGL-TR-78-0130	2. GOVT ACCESSION NO. / 3. RECIPIENT'S CATALOG NUMBER
(6) 4. TITLE (and Subtitle): PROBLEMS IN MODELING THE EARTH'S TRAPPED RADIATION ENVIRONMENT.	5. TYPE OF REPORT & PERIOD COVERED: Interim Report 1 Oct 1977–30 Sept 1978
	6. PERFORMING ORG. REPORT NUMBER: Scientific Report No. 1
(10) 7. AUTHOR(s): James I. Vette, King W. Chan, Michael J. Teague	8. CONTRACT OR GRANT NUMBER(s): PRO-00828-78 do not use
9. PERFORMING ORGANIZATION NAME AND ADDRESS: NASA-Goddard Space Flight Center, Greenbelt, MD 20771	10. PROGRAM ELEMENT, PROJECT, TASK AREA & WORK UNIT NUMBERS: (16) 62101F, 7601-12-AA (17) 12
11. CONTROLLING OFFICE NAME AND ADDRESS: Air Force Geophysics Laboratory, Hanscom AFB, Massachusetts 01731, Monitor/H. B. Garrett, Capt, USAF/PHG	(11) 12. REPORT DATE: Dec 1977; 13. NUMBER OF PAGES: 32
14. MONITORING AGENCY NAME & ADDRESS (if different from Controlling Office)	15. SECURITY CLASS (of this report): Unclassified (12) 33p.
	15a. DECLASSIFICATION/DOWNGRADING SCHEDULE: N/A

16. DISTRIBUTION STATEMENT (of this Report)

Approved for public release; distribution unlimited.

17. DISTRIBUTION STATEMENT (of the abstract entered in Block 20, if different from Report)

18. SUPPLEMENTARY NOTES

19. KEY WORDS (Continue on reverse side if necessary and identify by block number)

Trapped fluxes
Electrons
Protons
Radiation belt
Dosage

20. ABSTRACT (Continue on reverse side if necessary and identify by block number)

This report documents the status of the trapped radiation models presently available from NASA. Problems regarding energy, spatial, and temporal coverage are discussed in detail. Suggestions are made as to which type of measurements are most needed for model improvements.

DD FORM 1 JAN 73 1473 EDITION OF 1 NOV 65 IS OBSOLETE

Unclassified

SECURITY CLASSIFICATION OF THIS PAGE (When Data Entered)

409 578

Contents

Illustrations

Illustrations

Tables

Problems in Modeling the Earth's Trapped Radiation Environment

1. INTRODUCTION

The purpose of this report is to highlight for AFGL the problems encountered in modeling the terrestrial trapped radiation environment for the past 14 years, and to indicate steps that could be taken to improve their accuracy. Since this modeling activity has been confined principally to the energetic electrons and protons, the following remarks will apply to the energy ranges between 40 keV and 5 MeV for electrons, and between 100 keV and 170 MeV for protons. The intent here is not to present a review of the characteristics of the latest models produced by the National Space Science Data Center (NSSDC), since these are amply documented in the first 12 references listed at the end of this report. However, examples from these models will be utilized along with other data to demonstrate the theme of this discussion. In order to avoid a duplication of the numerous figures and tables of those references to clarify some statements in this report, copies of these 12 references will be provided as attachments. At the conclusion of this report, it is hoped that AFGL will have a better understanding of the complexity of this modeling activity, and can understand what must be done in order to significantly improve existing models through its Program to Measure and Model the Energetic Particle Environment. The inherent errors in the models will be discussed in general terms since specific errors depend strongly on the particular uses of the existing models.

At the outset it must be recognized that there are a large number of temporal and spatially varying phenomena which affect the energetic particle populations in the trapping region of the earth's magnetosphere. Specifically, the past and present state of the interplanetary medium in near-earth space (the solar wind velocity, density, and temperature, the interplanetary magnetic field (IMF), including the Z component, and passage of interplanetary shocks) play a major role in producing excitation in the magnetospheric cavity in the form of magnetic storms and substorms, which give rise to particle injection and acceleration mainly through the plasma sheet in the geomagnetic tail. Boundary currents in the magnetopause produce alterations in magnetic field within the cavity as well as do the injection of lower energy plasma from the ionosphere, the geomagnetic tail, and the interplanetary medium to form the ring current in the spatial region between 2 and 6 earth radii. In addition, electric fields produced by convection of IMF past the earth and through plasma instabilities within the cavity affect the motion of lower energy particles and contribute to acceleration and diffusion of the more energetic particles. The literature is rich in the description of these many complex phenomena and even a brief review of them is beyond the scope of this summary. A copy[1] is also attached since it is a recent survey of the trapped radiation by the modeling group at NSSDC and contains references to the recent literature on this subject.

We will confine our discussion to the following quantities. The basic measurements obtained by energetic electron and proton instruments flown on satellites are either the omnidirectional or unidirectional flux (pitch-angle distribution) within certain energy intervals or above nominal threshold energies. In the strict sense, the omnidirectional flux is the number of particles, of specified type and energy range, that pass through a spherical surface with a unit cross-sectional area in a unit time and is expressed most typically as the number of electrons (or protons)/ cm^2-sec with the appropriate qualifiers on the energy range observed. Most practical detectors fall short of this ideal geometry but differ from the more directional instruments which are sensitive to particles only in a narrow angular range. For purposes of this report we consider directional detector systems as those with a solid angle of less than 0.06 steradians, while omnidirectional detectors are those sensitive over substantial fractions of the 4π steradians of the sphere. Because a spacecraft and its systems provide a significant amount of shielding, the most ideal geometry for such omnidirectional measurements are 2π steradian detectors. Because of the nature of the trapped radiation, this geometry is equivalent to the spherical 4π steradian detectors. Directional trapped radiation detectors

---

1. Chan, K.W., Sawyer, D.M., and Vette, J.I. (1977) The trapped radiation population, in The Trapped Radiation Handbook. Eds. J.B. Cladis, G.T. Davidson, and L.L. Newkirk DNA 2524 Change 5, Defense Nuclear Agency.

must be referenced to some spatial axis which is usually the actual magnetic field observed by a magnetometer on the spacecraft. The spatial position of either type of instrument must be known during the accumulation of particle counts over a small period of time, and this requires the use of some reference coordinate system. Consequently, obvious independent variables of the flux function are the positional coordinates, the energy coordinate, an angular coordinate for directional systems, and time, since it is known from observations that time variations are very important. It is the variation of the observed fluxes with these variables, coupled with the physical characteristics of the orbiting instruments (particle energy response, angular response, and dynamic range for counting), that will be used to describe the inherent problems in obtaining suitable models of the energetic trapped radiation environment. The extremely large volume of space which must be observed is the dominant factor responsible for the poor sampling that has characterized the basic data used to produce existing models.

2. COORDINATE SYSTEMS AND SPATIAL GRADIENTS OF PARTICLE FLUXES

Although the trapping region of the magnetosphere is a time varying volume of space, reasonable time-averaged limits of the region are within 11 R_e of the earth and restricted to $\pm 70^0$ in geomagnetic latitude. Since the energetic trapped particles represent a small energy density relative to the energy density of the magnetic fields within this region, the particle motions are confined to gyration, bounce, and drift on these magnetic field lines. In addition, the density of the earth's atmosphere restricts energetic particle populations to the region above 1.15 R_e; the radial gradient becomes very steep below 1.2 R_e.

To appreciate the vastness of the trapping region, consider that this volume must be broken into cubical cells of 0.1 R_e on a side at radial distances between 1.2 and 7 R_e, and 0.2 R_e between 7 and 11 R_e, in order to properly account for the spatial gradients of the observed time-averaged fluxes. The reason for such cell sizes will become apparent later in the report. A simple calculation reveals that if a strictly geographic coordinate system is used, 1.9×10^6 such cells are involved. To provide a reasonable energy spectral distribution about 12 electron and 20 proton energies, must be used. Since the observed omnidirectional fluxes are observed to vary from cosmic ray levels of order $1/cm^2$-sec to order $10^8/cm^2$-sec for the lowest energy particles considered, a straight forward geometrical approach might require a storage size of some 10^7 to 10^8 bytes. This would clearly be cumbersome, if not totally impractical, even with present day computer technology.

Consequently, the modelers must use some physical understanding of the trapping phenomena as well as data compression techniques in order to produce a model that can be used in a practical manner. The first trapping region of the magnetosphere that was understood was the inner zone or Van Allen belt. Except for perturbations caused by extremely large magnetic storms or by artificial injections from nuclear detonations, the ordering of particle fluxes in this region was shown to be adequate by using the two-dimensional B (scalar magnetic intensity) and L parameter system introduced by McIlwain and computed using the harmonic representation of the internal geomagnetic field. Other coordinate variables derived from these two have also been useful and in the practical models produced, the ratio of the magnetic field at the point of measurement to that at the geomagnetic equator of the same field line, B/B_o, along with L, have been used as the basic system. The great advantage of such a system is that it is two-dimensional instead of three-dimensional; this alone results in a reduction of the number of spatial cells required by more than a factor of 10^2. In addition, the use of B/B_o provides a rapid recognition of positions near the geomagnetic equator on each L shell.

In the gross sense the major error produced by the choice of a two-dimensional system is at very low altitudes for electrons, where longitudinal asymmetries are observed because of the displacement of the dipole moment from the center of the earth, and of the electron precipitation produced by atmospheric scattering. However, flux levels at altitudes below 400 km are small enough that only highly radiation sensitive devices such as man and film require additional concern and, even here, low altitude orbit satellites perform an average over longitude in several days.

As one moves to the outer electron zone, it is apparent that a third spatial coordinate is needed for the region above 5 R_e even for long-term, time-averaged fluxes. Although it is understood distortions of the internal geomagnetic field are produced by the ring, magnetopause, and geomagnetic tail currents, a more physically meaningful coordinate system using these external fields is not practical nor were there good external field models available in the early days of modeling this environment. In addition, nonadiabatic time variations of the particle fluxes (discussed later) are known to dominate the region above 2 R_e. Continual and discrete flux increases following magnetic storms to distances as low as 1.5 R_e preclude the use of external field models to order the trapped fluxes effectively. The third spatial coordinate adopted for model work has been local time, since it is the best one to account for the distorted magnetic field with respect to the sunward and anti-sunward asymmetry, which alters particle motion over a much larger volume of space than that where longitude is a better third spatial coordinate. Since the dominant use of the trapped radiation models has been for satellites which orbit

for long enough periods to effectively average both time and local time variations, all practical models have contained local time-averaged fluxes. This results in a two-dimensional spatial matrix for storing the models in a digital computer for all parts of the trapping region.

To demonstrate some of the problems related to the spatial flux variations and the coverage of the trapping region by various satellites, we employ B/B_o, L, and the local time, Φ, as the spatial coordinates. Some of the graphs referred to in the references use B instead of B/B_o, but this should not present any problem to the readers. The omnidirectional time-averaged flux is then a function of these spatial coordinates and of the energy of the particle namely, $J(B/B_o, L, \Phi, E)$. Because of the variations of the flux with energy, it is necessary to consider a number of energies (~ 10) to provide numerical models which can then be interpolated adequately to obtain the energies of interest for a given application. The flux on a given field line (L shell) varies from some peak value at $B/B_o = 1$, the geomagnetic equator, in the range of 10^8 to 10^3 depending on particle and energy, down to about 1 particle/cm^2-sec at the atmospheric cutoff. With such large fluxes, it is more appropriate to express radial gradient in the form of the logarithmic gradient, for example

$$\frac{d}{dL} (\ln J) = \frac{1}{J} \frac{dJ}{dL} \quad .$$

For inner zone electron fluxes above 1 MeV near the inner radial boundary, this logarithmic gradient is typically $190/R_e$. Consequently, choosing a cell size with a radial dimension of 0.1 R_e can still produce large errors in computing the omnidirectional flux from a numerical model with fluxes given at various matrix points. At L values around 2.0, this gradient is typically $5/R_e$. To obtain a reasonable grid size for the models, in view of radial gradients, the L space is typically divided in 0.1 R_e segments from $L = 1.2$ to 7.0 and to 0.2 R_e for L values above 7.0. The B/B_o intervals are chosen by considering the omnidirectional flux at the equator and assigning about three B/B_o intervals per decade of flux. Consequently, if the equatorial flux is 10^7 particles/cm^2-sec for a given L shell, about 21 intervals will be chosen. Using this approach, the total number of B/B_o, L, and E grid points in the models is about 7,000 for both particles. Assuming 4 bytes are necessary for the flux at the grid points, the models are stored in about 28,000 bytes.

With the exception of the region covered by geostationary equatorial satellites, it is very difficult to obtain a measure of the local time variation of the trapped flux. The reason for this difficulty is that the sampling of all values of local time require several months to one year in most orbits. Consequently, the removal of

inherent time variations through averaging is not easy and local time variations can still be masked by these time variations. However, a geostationary spacecraft samples all values of local time within 24 hr and so the local time variations can be ascertained fairly accurately. The results obtained by Paulikas and Blake on ATS 1 are shown in Figure 22 (p 60)[2] for various energy electrons. The ratio of maximum to minimum varies from about 1.7 at 300 keV to 3.2 at 1.9 MeV for this data. The results obtained in the construction of outer zone electron model AE-4 indicate that these diurnal variations are not extractable below L = 5.0 and tend to build up at least until one gets to L = 8.5. It is difficult to determine this variation at higher L values and the average variation can get as large as a factor of 15.

Until more definitive results can be determined by much greater coverage, the averaging over local time is the only practical approach for presenting a useful model. Most satellites sample all values of local time during the course of orbiting for several years, consequently a local time averaged flux is the appropriate form to be applied for accumulated fluence determination. However, in comparing instantaneous fluxes from two measurements that differ only in their local time variable, large differences can be expected.

3. SATELLITE COVERAGE OF THE TRAPPING REGION

The volume of the trapping region is so large that adequate coverage to monitor energetic particle populations has never been practical. Since each satellite is confined to a particular orbit, no one satellite has ever provided a good sampling of all the regions for which measurements should be made. Because of the general character of the trapped radiation, the most complete coverage by a single satellite would be one in an equatorial orbit with an apogee and perigee that covered the trapping region; such a spacecraft would have to have a unidirectional particle detection system that was capable of measuring the complete equatorial pitch angle distribution over the desired range of energies.

To demonstrate that the lack of spatial coverage for any specific epoch is a very real and practical problem, a series of figures have been prepared to show this coverage for the current models that have been produced by NSSDC. These current models are summarized in Table 1. Proper documentation for AEI-7 has not been issued although the computer decks have been distributed. A discussion of the need for this latter model on an interim basis (hence the use of the I in the model designation) will be discussed in Section 6.

---

2. Vette, J.I., Ed. (1971) Models of the Trapped Radiation Environment - Volume VII: Long Term Time Variations, NASA SP-3024.

Table 1. Current NSSDC Radiation Environment Models

Name of Model	Particle and Energy Range	L Range	Remarks
AE-4	Electrons 0.04 - 4 MeV	2.8 - 11.0	Flux values for epoch 1964 and 1967 corresponding to solar minimum and maximum conditions. Solar cycle effects only occur between $2.8 \leq L \leq 5$. Energies above 4 MeV are strictly extrapolations, and data above 1.9 MeV did not have proper calibration. Data used in making model are shown in Table 1 of Reference 7 (p. 31).
AE-5 (1975 projected)	Electrons 0.04 - 4 MeV	1.2 - 2.8	Flux values for Oct. 1967, but Starfish residue subtracted and solar cycle effects used so projected valid epoch is 1975, corresponding to solar minimum conditions. Data sets used in making model are shown in Table 3 of Reference 9 (p. 57) with Starfish model of Reference 8 used in subtraction.
AE-6	Electrons 0.04 - 4 MeV	1.2 - 2.8	Flux values for Oct. 1967, but Starfish residue subtracted.
AP-8	Protons 0.1 - 400 MeV	1.17 - 6.6	Model has both solar minimum and maximum values; these changes only occur at low altitudes. Data used in making model are shown in Table 1 of Reference 12 (pp. 19-22).
AEI-7	Electrons 0.04 - 5 MeV	2.8 - 11.0	Interim model with upper and lower limit for energies above 1.5 MeV to account for ATS 6 data at 3.9 MeV and OV1-19 data up to 5 MeV. Model is interim until discrepancies between Azur data at 4.5 MeV and OV1-19 data can be properly studied. At energies below 1.5 MeV, this model is same as AE-4 in the outer zone for solar maximum.

Figures 1 and 2 show the B/B_o - L coverage of the data utilized in constructing the electron and the proton models, respectively. The magnetic equator is represented by the axis of $B/B_o = 1$ or $\lambda_m = 0^o$. The entire area included by the 100 km-cutoff curve and the equatorial axis is accessible to spaceborne experiments. The regions, in which data from only one spacecraft and from more than one spacecraft were available, have been shaded separately. The blank area indicates no data coverage, and in the case of AP8 (Figure 2) one should note that L = 6.6 is the model cutoff.

With some 24 spacecraft used for AP8 and 13 for AE-4/-5 models, and considering the accumulation of coverage over a period of 10 years for all energies, it is surprising to note that there are still gaps and regions not well monitored. If we had displayed the cross-section of a month of time and a given energy interval, the spatial coverage would have been far from complete.

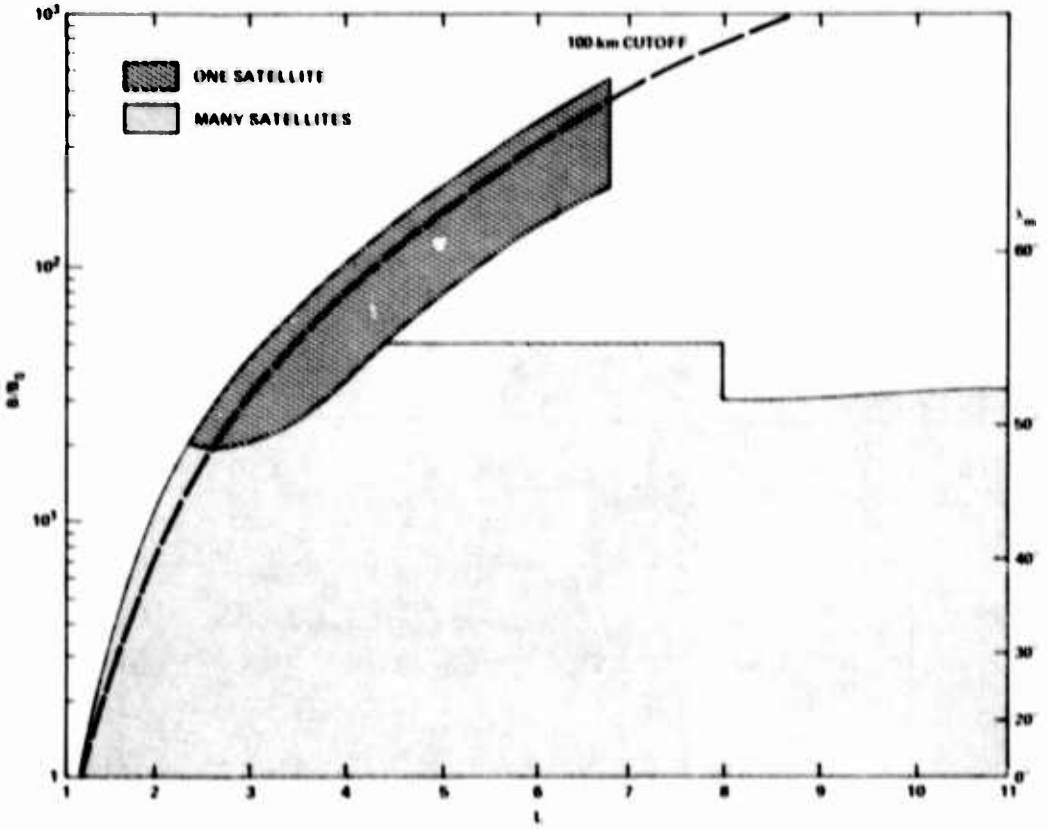

Figure 1. B/B_o - L Coverage for Experiments Used in Constructing the AE-4 and AE-5 Models. The area shaded for one satellite is covered by the polar orbiter Injun 3

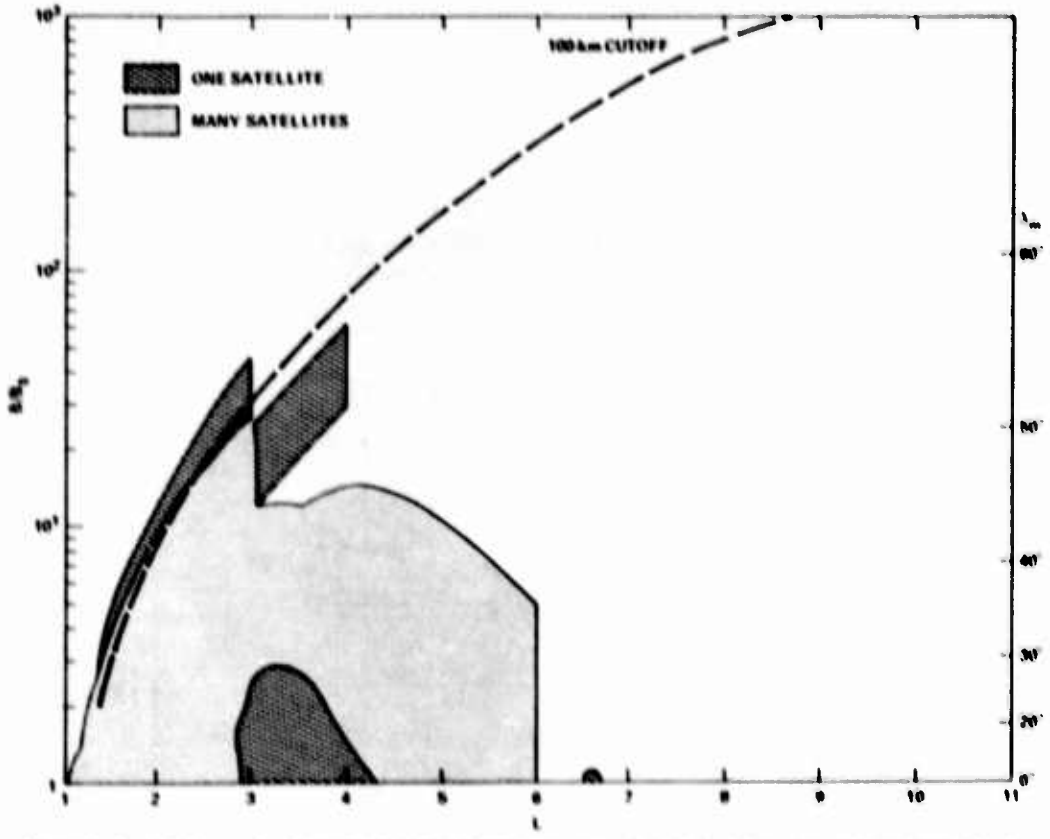

Figure 2. B/B_0 - L Coverage for Experiments Used in Constructing the AP-8 Model. The model and the data used have a cutoff at L = 6.6

A summary of the energy-time coverage of data used in the various models is shown in Figures 3 and 6. In each of these diagrams, the energy intervals of the particle channels are marked by the vertical bars, and the nominal energy of the threshold channel is indicated by a single upward arrow. The time span of the data channel used in modeling is represented by the length of the horizontal bar together with the spacecraft designation. By inspection of these figures, it is immediately apparent that the high-energy data, >2 MeV for electrons and >100 MeV for protons, are largely lacking in the data base of current models. Furthermore, there have been very little data available between 1959 and 1961. Figure 6 is the planned data coverage to be used for Model AE-7 and will be discussed in detail in Section 6.

Returning to the in-situ measurements by an individual satellite, the sampling limit of a given orbit can be readily illustrated. For the polar orbiters with apogee about 4,000 km (for example, OV3-3, AZUR), the equatorial region of all $L > 2.0$ is not covered. An example of the actual data acquired by AZUR at three L-values have been shown in Figure 43 (p 73).[2] It is obvious that these polar orbiters

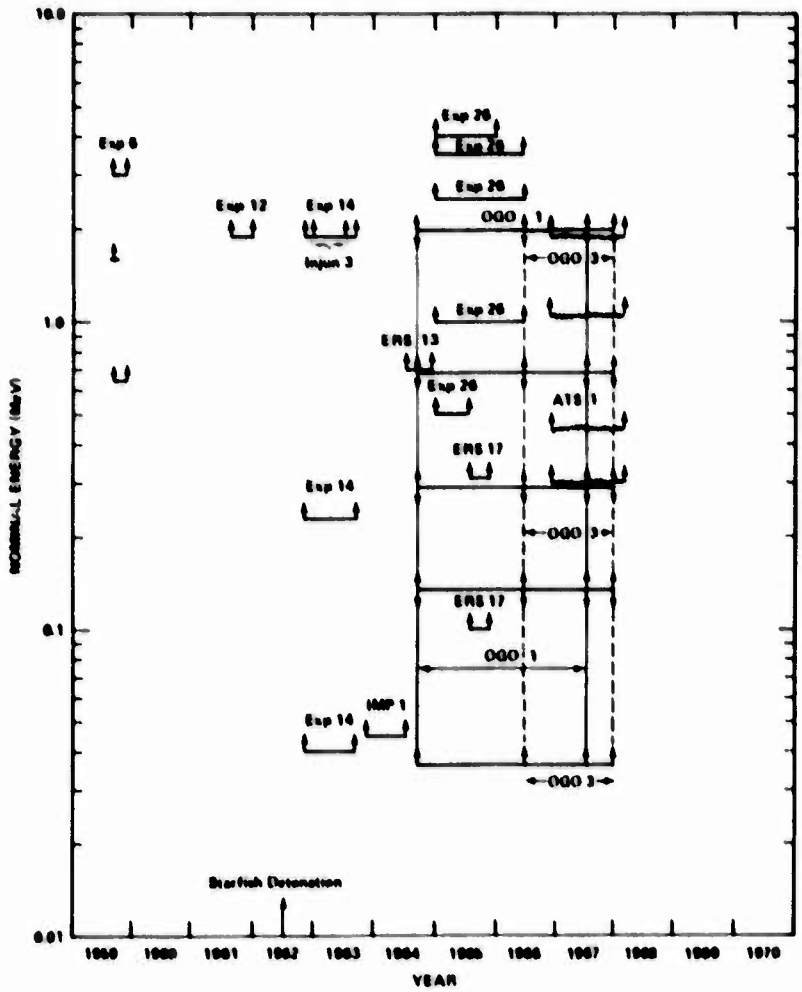

Figure 3. Energy - Time Coverage for Experiments Used in Constructing the AE-4 Model. The nominal energy of threshold detectors are shown with the upward pointing arrows and the energy bands of the interval detectors are presented by the vertical bars. The time span of the data used is indicated by the length of horizontal bars. The Starfish Detonation event is marked on the time axis

can contribute only about half of the B/B_o range required by the model and no equatorial measurement can be made for L values above 2.0.

On the other hand, the high-altitude, low-to-mid-latitude satellites, such as OGO-3 and OGO-5, are restricted by the poor time-coverage of the trapped radiation zones. With an initial apogee of about 23 R_e, these spacecraft can sample a given L-value only twice every two days. This kind of data sampling will miss

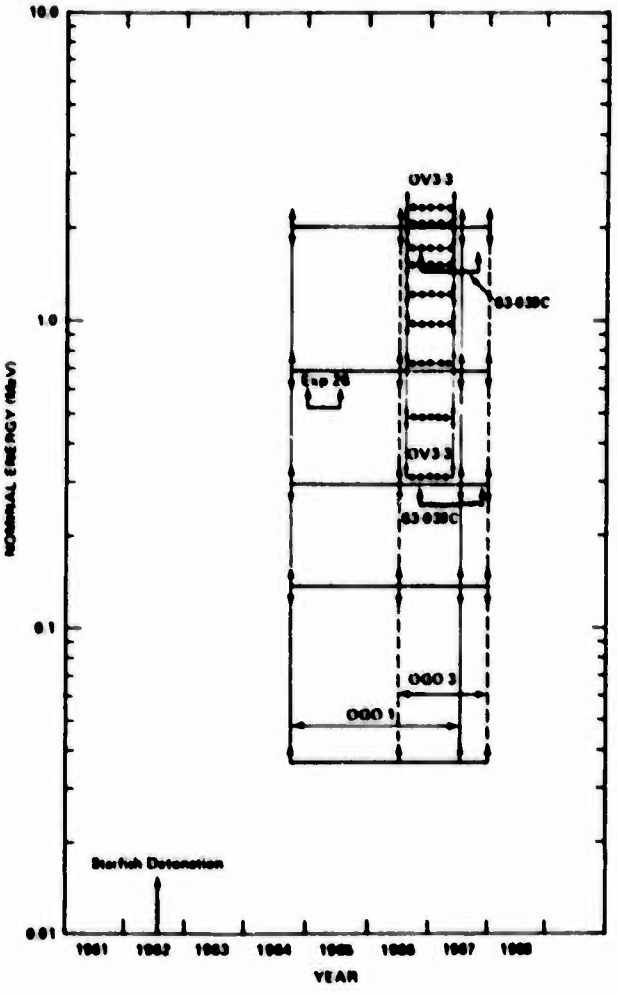

Figure 4. Energy - Time Coverage for Experiments Used in Constructing the AE-5/-6 Models. Notations are the same as in Figure 3

most of the predominant short-term temporal variations in the outer zone, which will be further explored in the following sections.

Detailed spatial and spectral coverage have been given in most of the model documents. Readers can refer to Figures 96 through 128 (pp 118-146)[3] for specific examples. General comments on the near-term outlook on this area and recommendation for future measurements will be discussed in Sections 6 and 7.

3. Sawyer, D.M., and Vette, J.I. (1976) AP-8 Trapped Proton Environment for Solar Maximum and Solar Minimum, NSSDC/WDC-A-R&S 76-06.

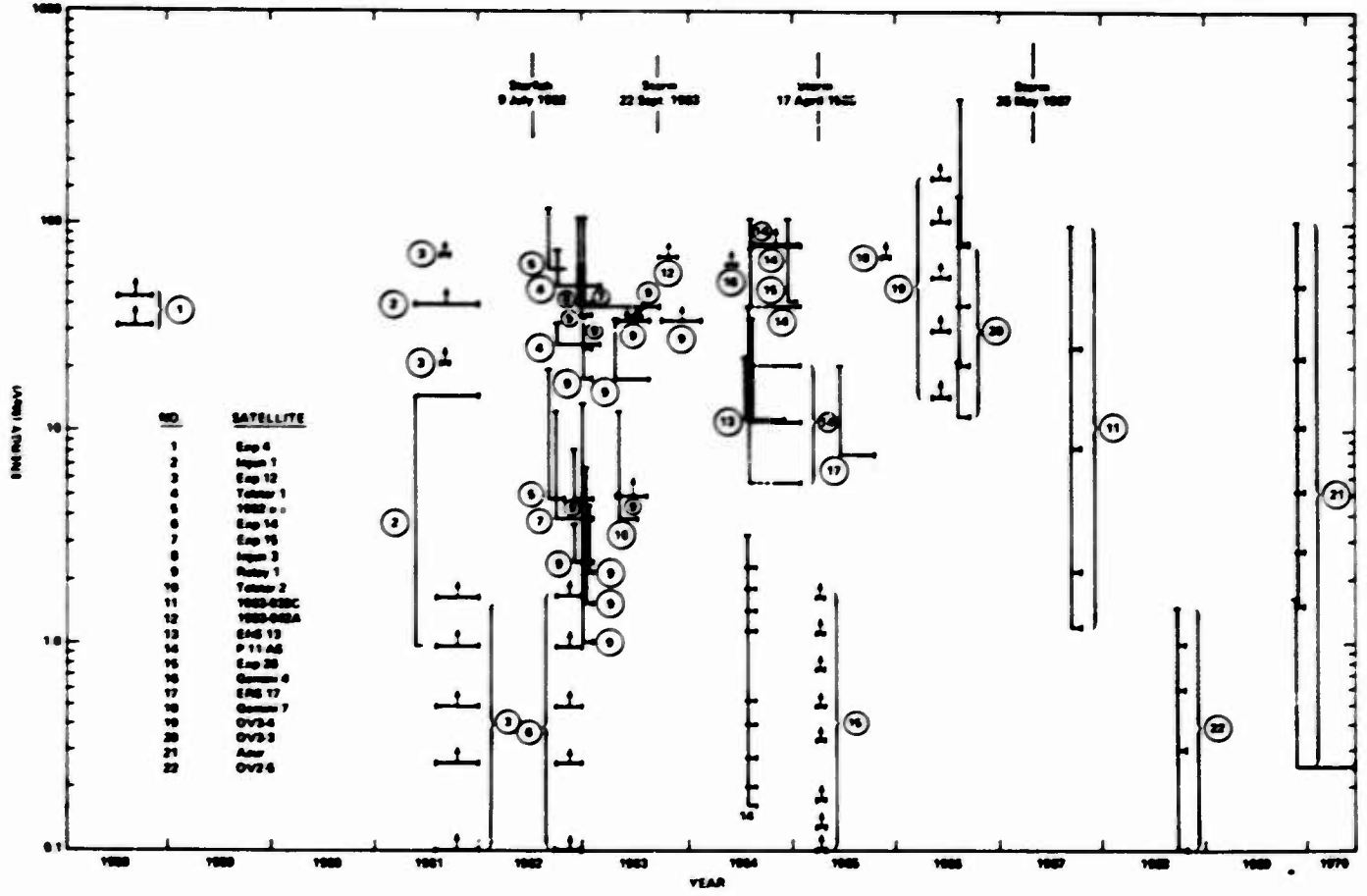

Figure 5. Energy - Time Coverage for Experiments Used in Constructing the AP-8 Model. Notations are the same as in Figure 3. Three major magnetic storms occurred in 1963, 1965, and 1967 are marked in addition to the Starfish event

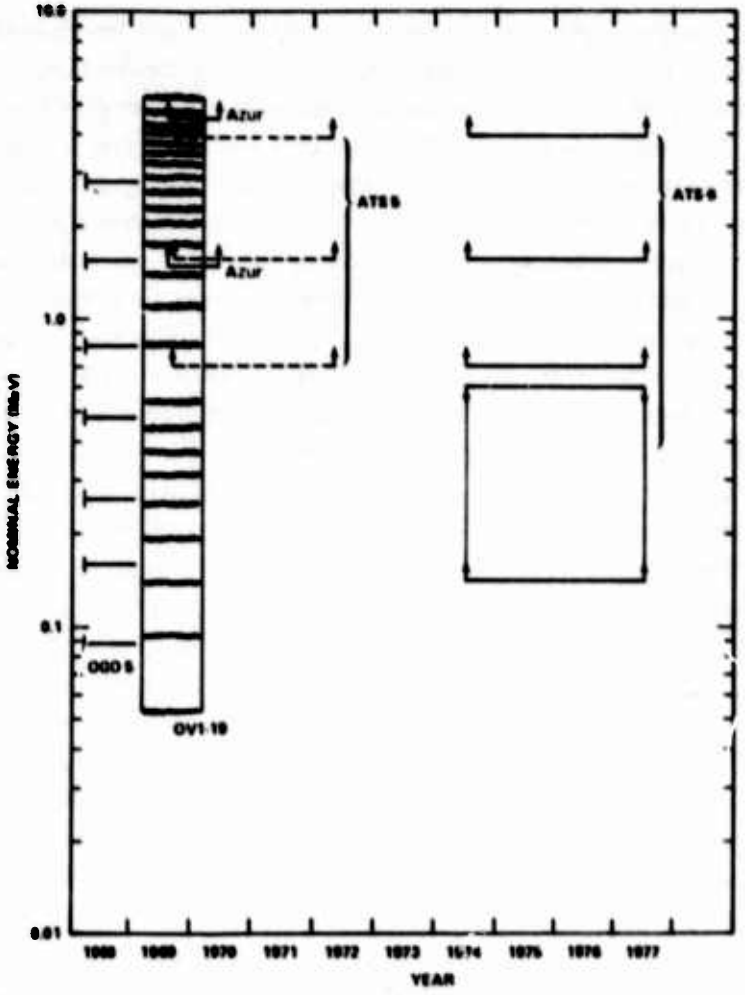

Figure 6. Energy - Time Coverage for the New Data to be Used in Constructing the AE-7 Model. Notations are the same as in Figure 3. Since the AE-7 model has not been completed, this figure is only a tentative graphic illustration of a plan

4. SPECIAL VARIATIONS, THE CALIBRATION OF DETECTORS, AND OTHER DETECTOR PROBLEMS IN MODELING

The large spatial gradients encountered throughout the trapping region make the coverage problem a difficult one since an impractically large number of orbits would normally be required. Spectral variations produce another problem that affects the modeling efforts. The majority of the data used in producing trapped radiation models has been obtained from scientific satellites in which the emphasis has been on understanding the dominant physical phenomena in any given region at

a given time. Surprisingly, the quantitative response of the instrument to the trapped particles has not been the important factor in understanding the physics of region; so whether an electron detector is predominately sensitive to all electrons about 1.6 or 1.9 MeV makes little difference in the ensuing data analysis and physical interpretation. However, the average energy spectrum in the equatorial geostationary region gives approximately a factor of 4 difference in the omnidirectional flux for these two energy levels. In using data from many satellite-borne experiments, a quantitative comparison of different detector systems is an important factor in obtaining the best value of the flux. This requires that the energy sensitivity of a detector system be known with reasonable accuracy. Since electrons scatter quite readily in the shielding material employed with these detectors as well as with spacecraft mass, the energy response can best be obtained through extensive calibration employing sources of known intensities and energies. There have been many electron detector systems flown which have never been properly calibrated. This results in considerable error since the spectral distribution of trapped electrons varies greatly in time and space. Electron detectors that measure energies mainly below 1 MeV can be calibrated by many available sources and accelerators, and even reasonable estimates can be made by calculations if the electronic discriminators are known to be set at reasonable levels to detect most of the energy lost by the electron in the sensitive volume of the detector. However, for energies above 1 MeV, a detailed calibration is an absolute necessity. The ATS 6 system of Paulikas, Blake, and Imamoto[4] referred to in Figure 7 certainly meets the level of detail required and covers an adequate energy range. We have encountered a recent example where comparisons with these ATS 6 detectors and others claiming an effective threshold of 2 MeV show a factor 15 discrepancy in the average flux. It has been our belief that most energetic electron detectors above 1 MeV have never been adequately calibrated; therefore, there is still considerable controversy about the best flux values in this energy region. Proton detector systems have usually measured particles within an energy interval that is too large for it to be considered a differential energy analyzer. Although many of these systems have not been properly calibrated in the past, a calculated energy response is generally more accurate than for electrons. Consequently, the comparison of various instruments has been somewhat more favorable although extensive calibrations are still necessary to determine flux levels to accuracies better than a factor of two.

---

4. Paulikas, G.A., Blake, J.B., and Imamoto, S.S. (1975) ATS-6 Energetic particle radiation measurement of synchronous altitude, IEEE Trans. on Aerospace and Electronic Systems AES-11:1138-1144.

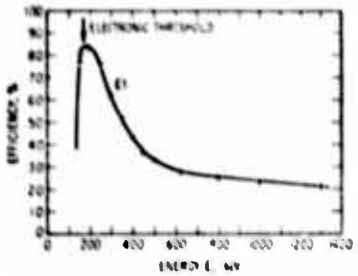

Efficiency of detection of electrons in the $E1$ channel. This channel has a nominal energy sensitivity of 140-600 keV. Sensitivity of this channel below the nominal electronic threshold is associated with the finite noise of the detector.

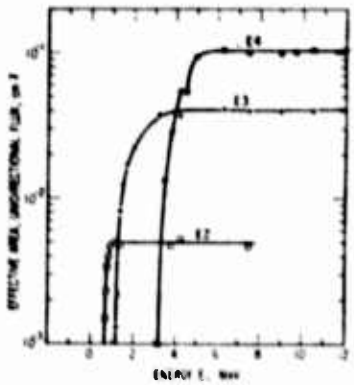

Effective area of the $E2$, $E3$, and $E4$ electron channels as a function of electron energy. This effective area, when integrated over the angular response of the detector, yields the omnidirectional geometric factor.

Channel	Passband or Threshold (MeV)	ϵG
E1	0.140 - 0.600	.115 cm^2 - sr
E2	0.700	.00349 cm^2
E3	1.55	.0176 cm^2
E4	3.90	.0688 cm^2

Figure 7. Energy Calibration Data for the ATS 6 Detectors. E2, E3, and E4 are threshold detectors. E1 is interval detector (After Paulikas et al, Ref. 14)

Returning to electron detectors, it has been our experience that the interpretation of threshold detectors by various investigators in terms of quantitative flux levels is somewhat inconsistent. This inconsistency can range up to a factor of four in terms of the absolute value of flux in certain regions of space. However, whenever the energy response curve has been available to us, this difficulty has been removed by folding the final model spectrum with the response curves in a consistent manner to determine what the proper conversion factor from counting rate to flux should be. For the higher energy threshold detectors this factor is spectrum dependent, therefore, it is also spatially dependent. Of course we have had no valid way of establishing the accuracy of the energy response curves provided along with the particle data. Therefore, the final flux values for the models are a subjective best estimate. However, it has been our practice to illustrate fairly completely the differences between the experimental flux values obtained by

each experiment and the model values. A scanning of the most of the references cited will demonstrate this detailed comparison.

Directional detectors have presented several difficulties for incorporating the results into the models. These instruments have either provided the flux perpendicular to the magnetic field line, or given a measurement at a particular pitch angle at some point on the field line. In order to obtain the omnidirectional flux, the complete equatorial pitch angle distribution on each field line must be determined. Consequently, each pitch angle measurement must be translated to the equator using adiabatic theory. A typical equatorial pitch angle distribution is shown in Figure 8. Near the atmospheric cutoff one can see that the slope becomes quite steep. This results in various errors because the finite angular response of the instrument and the direction of instrument relative to the field line must be known fairly well. During injection events when there are large increases in the flux, this pitch angle distribution is known to change from the average or equilibrium values. Since one is effectively performing a different type of time averaging than with omnidirectional detectors, the final values might be different by as much as a factor of two. And, of course, it is not possible to obtain an

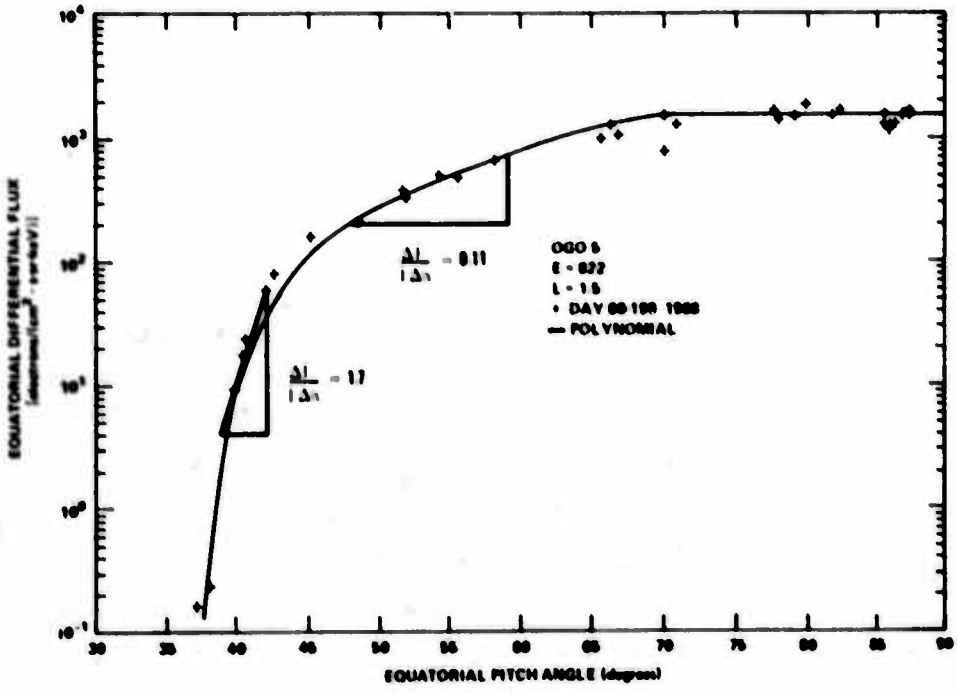

Figure 8. Equatorial Pitch Angle Distribution of 822 keV Electron Data From OGO-5. The polynomial curve is a best fit to the inner zone data base at L = 1.5. The slopes of the gradients, $1/j\ \Delta j/\Delta\alpha$, have the unit ($deg^{-1}$)

instantaneous comparison of an omnidirectional detector and a directional detector because they are measuring different portions of the particle population. Directional detectors require that the angular calibration be done more accurately than for an omnidirectional detector, and it has been our experience that the geometric factors of such systems as quoted by experimenter can change by a significant factor even after we have been processing the data for lengthy periods in the production of models. Generally, the geometric factors of omnidirectional systems can be calculated to better than a factor of two, so the modeler has some check on the quoted values, where as, the calculation of the effective geometrical factor for directional systems require a much more thorough knowledge of the construction of the instrument and do depend on the actual pitch angle distribution being observed. Directional detectors are extremely useful for scientific purposes but for the construction of time-averaged omnidirectional models, omnidirectional detectors present fewer problems. In addition, the effect of backgrounds produced by energetic particles that penetrate the shielding, which define, in many cases, the sensitive aperture, are not always able to be understood and removed properly.

Other problems that one must be aware of in using the data from particle detectors are the saturation effects. Since these effects can be produced by dead time within the sensor device such as in Geiger tubes, or in the discriminators that determine the minimum electrical pulse that will be counted, or in the counters or amplifiers, it is difficult to understand the various ways in which saturation effects manifest themselves. The valid dynamic range of an instrument system are usually not clearly defined to the modeler, and must be inferred by studying the final flux values or pitch angle distributions involved. As part of the calibration procedure of an instrument, the system should be exposed to large enough intensities of various energy particles to drive it into saturation. The saturation characteristics should be made available as part of the supporting documentation so that the modeler is not trying to incorporate measurements which are in gross error because of these effects. We can cite some very subtle effects that we have observed in data where the experimenter maintains the instrument was performing properly. It is very unwise to base a model on the data from one instrument; but because of the incomplete coverage in the four-dimensional space, B/B_0, L, E, time, we have had to do this in certain regions.

5. TEMPORAL VARIATIONS OF THE TRAPPED PARTICLE POPULATIONS

The most difficult problem encountered in producing models of the energetic particle environment results from the wide variety of time variations that are observed throughout the radiation belts. We will discuss these various changes

briefly because it is essential to understand why they pose such a problem, and it is useful to know the approaches that have been used in our modeling efforts. Since the most prevalent use for these models has been to determine the approximate radiation environment that new missions will encounter in a variety of orbits, the predictive aspect is a very important one. However, the data used to make a model are generally several years old before they are available for modeling the environment. Consequently, by necessity, predictions of 5 to 15 years are implied in the use of such models. This predictive aspect, coupled with complexity of the natural time behavior observed in the particle population, place a somewhat unknown limit on the accuracy of the models that cannot be overcome even with an extensive measurement program. Although detailed historical and performance data exist for companies listed on the New York Stock Exchange, the prediction of the price of the stock a decade, or even a year, in the future is known to be unreliable. With this analogy in mind, we will now outline the various time variations that have been handled in the production of the models to date, and point out some of the difficulties and the successes.

Serious modeling of the radiation belts really began following the Starfish detonation of 9 July 1962, because this man-made perturbation had serious effects on the operation of a number of spacecraft in orbit. The inner zone electron fluxes were dominated by the Starfish residue for several years, which is illustrated by a comparison of the radial profiles at the equator of AE-2 and AE-5 as shown in Figures 1-6 (pp 23-28).[5] The decay of these electrons was observed for at least 8 years and it was necessary to model this decay as a function of L and E in order to produce AE-5 1975 projected, where observations taken during 1964-1966 were extrapolated to 1975, and AE-6, which is extrapolated to 1980. Typical values of decay time are given in Figure 9 (p 44)[6] and vary from 50 to 370 days. Effects of the Starfish residue had to be taken into account up until June 1970 in small regions of the inner zone. This can be seen in by referring to Figure 24 (p 55)[6] where the cutoff contours for the Starfish residue are shown as a function of L and E. Consequently, both current models, AE-5 1975 projected (for solar minimum conditions) and AE-6 (for solar maximum conditions), for the inner zone have been derived by subtracting a decaying Starfish residue from data taken more than 10 years ago. It is apparent from the above terminology that a long-term solar cycle change for the inner belt fluxes can be inferred, at least for electron energies below 690 keV; values of flux change as a function of E and L are given in Figures 86-93

---

5. Hilberg, R. H., Teague, M. J. and Vetter, J. I. (1974) Comparison of the Trapped Electron Models AE-4 and AE-5 with AE-2 and AE-3, NSSDC 74-13.

6. Teague, M. J., and Stassinopoulos, E. G. (1972) A Model of the Starfish Flux in the Inner Radiation Zone, GSFC-X-601-72-487.

(pp 134-141).[7] The flux changes are typically a factor of 3; however, at higher energies no such change can be obtained because of the masking effects of magnetic storms.

The effects of magnetic storms below L = 2.4 can be seen in Figures 8-11 (pp 60-63).[8] The spectrum hardens during the storm enhancements, the total energetic electron content increases by factors of 3 to 5 for higher L values of this region, with much smaller effects in the heart of the inner zone. These enhancements are observable for 2-3 months and are definitely discrete events. Because the frequency of these inner zone events is no more than one to three a year, their effects cannot be handled well on a statistical basis. The quiet-time fluxes with solar cycle changes have been used along with an average contribution from three magnetic storms, so that the average inner zone flux represents a time-averaged one that might be realized over a period of 1 year. If one were able to measure the omnidirectional flux at one point in space and integrate this over time, the fluence would be:

$$F_T(E,\ B/B_o,\ L) = \int_0^T J(E,\ B/B_o,\ L,\ t)\ dt$$

and the time-averaged flux would be:

$$J = F_T/T \quad .$$

The omnidirectional flux of AE-5 1975 projected and AE-6 corresponds to that which would be expected to be obtained if T were approximately 1 year.

Time variations for outer zone electrons require a somewhat different treatment and the excursions during magnetic-substorm enhancements are one or two orders of magnitude larger than in the inner zone when considered as a relative change in the ambient flux. A good illustration can be seen in Figure 9 (pp 41)[9] where the time behavior is more complex at L = 5.0 than it is at L = 4.0. The approach that has been taken in the outer zone has been to use a statistical approach to describe the time behavior and to attempt to obtain a time-averaged flux. Here the averaging time needs to be about six months in order to expect the observed

---

7. Teague, M.J., and Vette, J.I. (1972) The Inner Zone Electron Model AE-5, NSSDC 72-10.

8 Teague, M.J., and Vette, J.I. (1971) Variation of the Electron Spectrum in the Inner Radiation Belt, September 1964 to Present, NSSDC 71-11.

9. Singley, G.W., and Vette, J.I. (1972) A Model Environment for Outer Zone Electrons, NSSDC 72-13.

fluence to approximate that computed with the model. Of course, the local time variation, which has been discussed earlier as a spatial variation must be removed. This has been done by performing a local time average of the flux at a given L value. To place these various time variations into perspective, let us review the situation in the equatorial geostationary orbit near the geomagnetic equator ($L = 6.6$, $B/B_o = 1$). The instantaneous excursions can be up to three orders of magnitude as shown in Figure 11 (p 56)[2]; this data set is fixed in local time at midnight so that local time considerations do not have to be unfolded. However, for other than commensurately orbiting spacecraft, it is impossible to avoid this unfolding process. As we have remarked in Section 3, the local time variations at $L = 6.6$, $B/B_o = 1$ range up to a factor of 3.2 at 1.9 MeV and larger variations can be expected at higher energies. A graphical example of this can be seen in Figure 22 (p 60).[2]

The solar cycle effects in the outer zone electrons seem to be confined to L values below 5.0 and must be inferred by studying the fluxes averaged over about one year. This effect is illustrated in Figures 30 and 31 (pp 62-63)[9] and can be seen to amount to maximum changes between a factor of 3 to 10, depending on the energy of the particle and the L value. Because of the large short-term time variations, it has not been possible to obtain an orderly change in the average fluxes as was possible in the inner zone. At any rate, the effects of solar cycle changes have been handled by producing models of both the inner and outer zone at epochs corresponding to minimum and maximum conditions (the maximum designation is only approximate, because data in 1969, the latest solar maximum, were not available for analysis when AE-4 and AE-5 were produced). Considering the magnitude of the flux changes and noticing the effects of magnetic storm enhancements in the inner zone and the local time effects in the outer zone, a more systematic model does not appear warranted.

Some recent work by Paulikas and Blake (private communication), utilizing their ATS 6 data and the energetic electron data of McIlwain from ATS 5, demonstrate quite clearly that at energies below 1.55 MeV there are no solar cycle effects in the equatorial geostationary orbit region. This is illustrated in Figure 9. During mid-1974 when ATS 6 was at 94°W and ATS 5 was at 105°W, the two different experiments were intercompared so that differences of energy thresholds and errors in geometric factors would not affect the results. It is readily seen that no systematic solar cycle effect can be ascertained even when yearly averages are employed. This is consistent with the results cited earlier where the same experiment on OGO 1 and OGO 3 were also intercompared in the same time period by Winckler. There is another characteristic that can be noted in Figure 9; the yearly averages for the electrons above 3.9 MeV exhibit a stochastic change that is about a factor of 3. Consequently, an inherent error in these more energetic electrons,

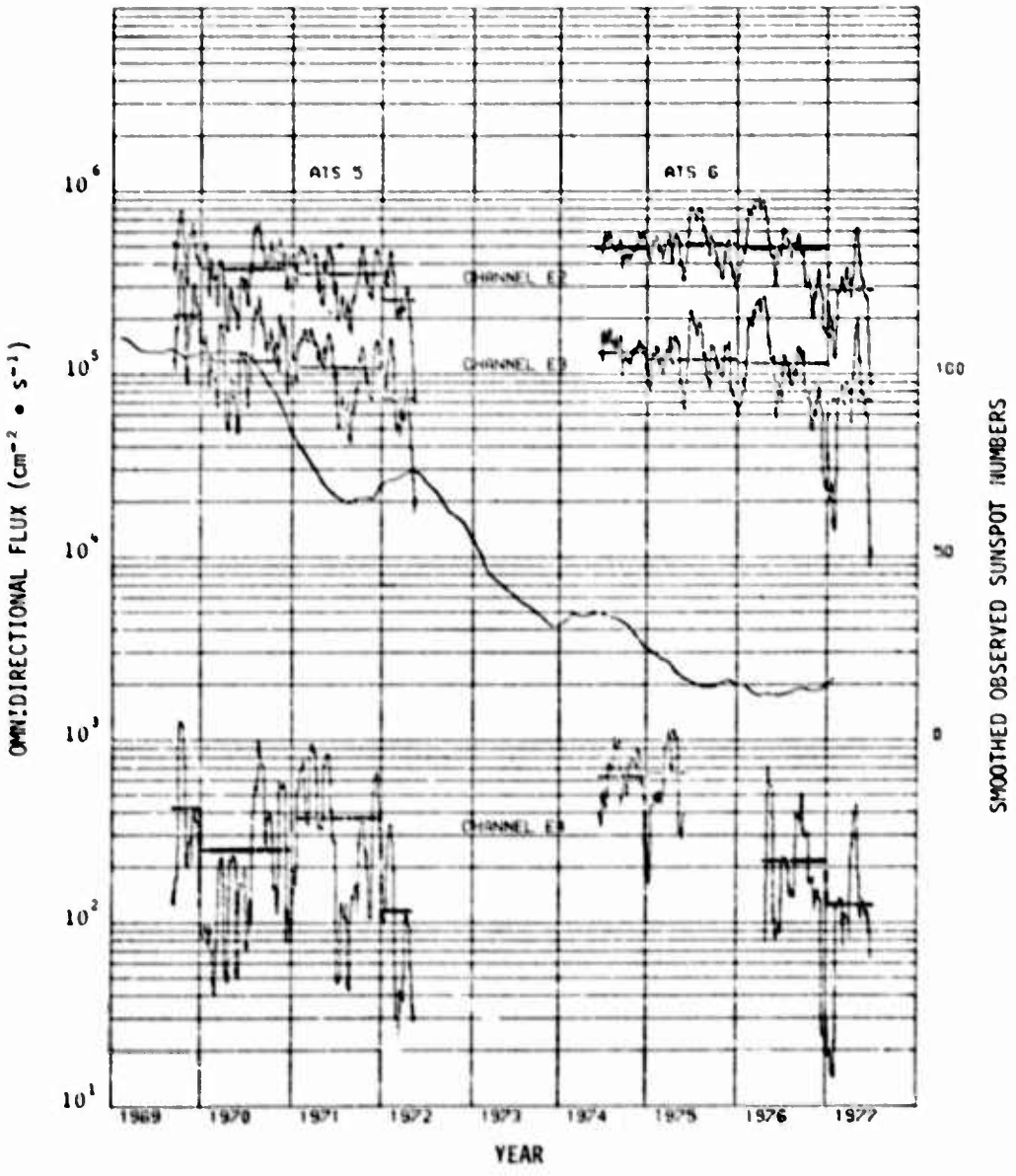

Figure 9. ATS 5 and ATS 6 Daily Flux Averages With Sunspot Numbers. (After Paulikas and Blake, private communication)

even for yearly averages, must be anticipated by those using models. New data will be required to determine if this effect is larger at other L values and at B/B_o values greater than 1.

Protons exhibit much smaller short-term variations than do electrons. This is amply demonstrated by looking at Figures 1-6 (pp 23-28).[3] Certainly the more energetic protons, say above 8 MeV, show very small changes while those below 1 MeV can show changes approaching a factor of 10. There have been two observations of large changes of protons above 35 MeV caused by magnetic storms that show both adiabatic and nonadiabatic changes. These are illustrated in Figures 1 and 2 (p 11)[10] and resulted in a reduction of the particle fluxes which recovered with time. The bump in the radial profile of 40 MeV protons discovered by McIlwain on Explorer 15 and Injun 3 and studied further by him on Explorer 26, provided some evidence of enhancements of energetic protons in a confined region of space. This particular distribution discussed by McIlwain can be seen in Figures 3 and 4 (p 11).[11] Since most of these types of changes are not predictable, occur infrequently, and, for nonadiabatic changes, require a year or more to recover, they are best handled by the user being aware that such departures from a stable model can be expected on rare occasions.

The long-term solar cycle behavior at low altitudes has been taken into account in AP8. The limited region of B/B_o, L space where this effect is observed can be seen in Figures 59-64 (pp 81-86).[3] These changes do result in flux level differences of more than an order of magnitude, but the altitude gradients are so steep in these regions that slight differences in the achieved orbits for such missions could result in equally large departures from the prelaunch expectations.

The time variations for trapped protons do not seem to place stringent limits on the accuracy of the fluxes in future models. However, to improve existing proton models, properly calibrated detectors providing complete enough coverage to obtain good time-averages will be required to reduce errors in future models.

6. THE NEAR-TERM OUTLOOK FOR ENERGETIC PARTICLE ENVIRONMENTS

The electron situation in the equatorial stationary orbit with energy range up to 3.9 MeV will be completely defined through the work of Paulikas, Blake, and Hilton (private communication) who will publish a detailed analysis of their ATS 1 and 6 results along with intercompared data from McIlwain's ATS 5 energetic

---

10. Lavine, J.P., and Vette, J.I. (1970) Models of the Trapped Radiation Environment-Volume V: Inner Belt Protons, NASA SP-3024.

11. Lavine, J.P., and Vette, J.I. (1970) Models of the Trapped Radiation Environment-Volume VI: High Energy Protons, NASA SP-3024.

particle experiment. This data, along with that from OGO 5, OV1-19, AZUR, and ISIS 2, is in the process of being analyzed to obtain a new outer zone model AE-7. This effort should be completed in about a year. Because of the length of time necessary to produce a properly analyzed model, it was necessary to issue AE1-7 on an interim basis to account for the new electron measurements about 2 MeV. Some of the changes from AE-4 that can be expected are illustrated in Figures 10 and 11 where the comparison of AE1-7 with some data are shown. The HI model is based on the OV1-19 analysis of Vampola. As one can see in Figure 10, there is basic disagreement between the AZUR and OV1-19 results. Both measurements were taken in the same time period.

The OV1-19 data of Vampola is presently being studied along with West's OGO 5 data to resolve the discrepancies with the AZUR data of Hovestadt. Clearly, the previous AE-4 model is low at energies above 1.5 MeV based on the ATS 6 data of Paulikas and Blake at the geostationary orbit. Since the calibration of these detectors, as shown in Figure 7, have been carried out very carefully to high energies, the validity of their results are unquestioned. In addition, their treatment of threshold detectors is identical to that which we introduced in AE-1 and their statistical analysis[2] is also identical to that which we introduced in the AE-3 construction and used in making AE-4 (a description of this technique can also be found in Ref 9). The major change from AE-4 is a hardening of the spectrum above an energy dependent on L. Whether the HI and LO limits used in AE1-7 will be adopted for AE-7 is not known. However, with the stochastic changes observed even in the yearly averaged fluxes shown in Figure 9 at 3.9 MeV such a feature seems justified. Part of the discrepancy between AE-4 and OV1-19 data at $L = 4.0$ may be a solar cycle effect. Solar maximum occurred in 1969 and the latest data used in AE-4 was early 1967.

Looking beyond the present analysis, the energetic particle data that will become available for modeling are shown in Table 2 where only currently operating spacecraft are given. We have only included those experiments where electrons of at least 0.8 MeV and protons of at least 8 MeV are measured. There are a number of other experiments on these spacecraft and ESA GEOS that measure lower energy particles.

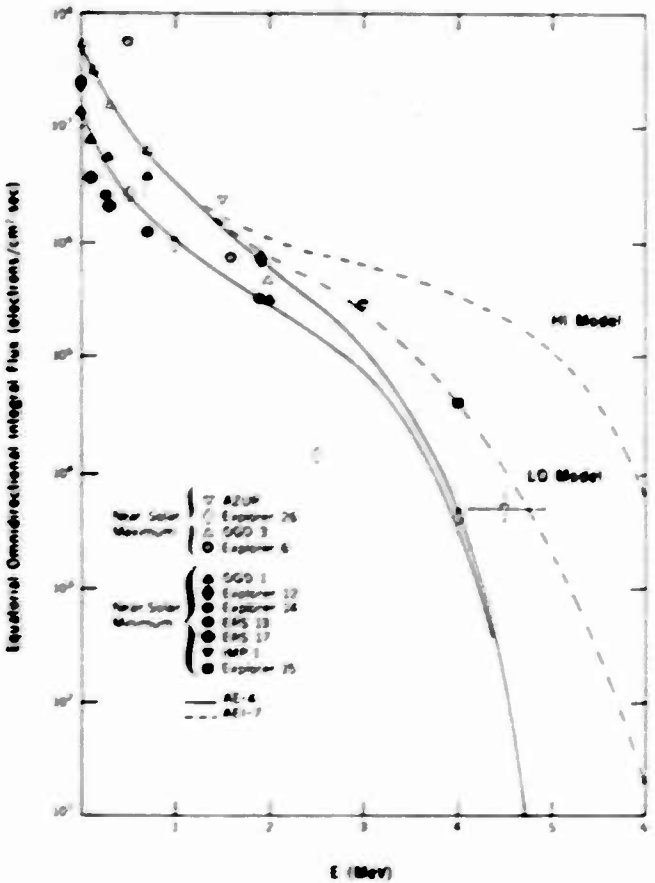

Figure 10. Comparison of AEI-7 Model Spectra With Various Data Set at L = 4. The HI model curve is mainly based on the OV1-19 observations from Vampola

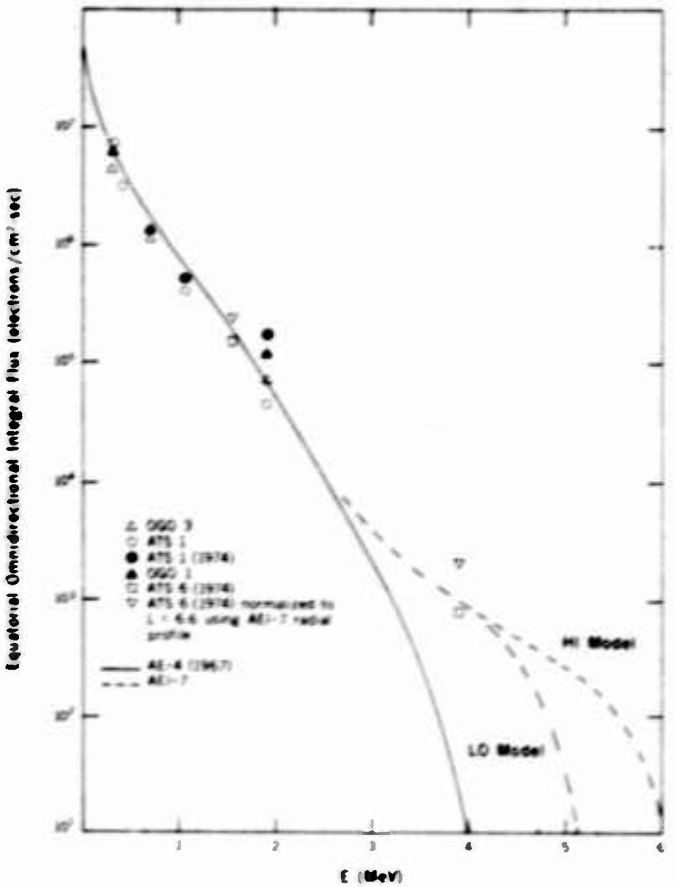

Figure 11. Comparison of AEI-7 Model Spectra With Various Data Set at L = 6.6. See text for detail

Table 2. Operating Spacecraft With Energetic Trapped Particle Experiments

Spacecraft	Investigator	L Range	Electron Range (MeV)	Proton Range (MeV)	Remarks
ATS 5	McIlwain	6.6 - 7.0	0.5 - 5	12 - 24	L value depends on longitude
ATS 6	Masley	6.6 - 7.0	0.05 - 1	0.3 - 250	
	Paulikas	6.6 - 7.0	0.14 - 3.9	2.3 - 90	
76-059A	Higbie	6.6 - 7.0	0.03 - 2.0	0.05 - 150	
77-007A	Higbie	6.6 - 7.0	0.03 - 2.0	0.05 - 150	
SMS/GOES	Sauer	6.6 - 7.0	> 2	1 - 500	Two spacecraft at any one time; L value depends on longitude
DMSP-F1	Blake	All	0.7 - 0.9	12 - 36	
ISEE 1	Williams	All	0.02 - 1	-	Two L measurements per 58 h
ISEE 2	Keppler	All	0.02 - 1	-	
ISIS 2	McDiarmid	All	0.02 - 2	0.15 - 28	
S3-2	Fennell	All	-	0.4 - 9	
S3-3	Vampola	All	0.01 - 1.6	-	
	Yates	All	-	3 - 100	

7. RECOMMENDATIONS FOR FUTURE MEASUREMENTS

In order to produce more accurate energetic particle environments in the future, the following recommendations result from the previous discussion:

(1) Use well calibrated omnidirectional instruments in orbits of opportunity and determine saturation effects before launch.

(2) Make special efforts to extend the electron energy range up to at least 8 MeV; in doing this attention should be given to discrimination against the contamination of penetrating protons in regions of the inner zone where their fluxes might be large relative to those of energetic electrons.

(3) Make special efforts to measure protons in the energy range from 100-600 MeV; contamination from energetic electrons and high Z particles should be discriminated against in designing such systems.

(4) Use digital counters and a digital spacecraft data system.

(5) If a single orbit for trapped flux measurements could be chosen, select an equatorial orbit with about 1000 km perigee and 40, 000 km apogee altitude and use directional instruments that can obtain the complete equatorial pitch angle distribution over the energetic particle spectrum. A spinning spacecraft with the spin axis normal to the orbit plane is ideal in this case; in addition, selecting a 12 hr commensurate orbit might greatly aid in the data acquisition coverage.

(6) Insure that resources are available to process all the acquired data to the point where engineering corrections are made, saturation effects are removed, periods of suspect instrument performances and bad data are deleted, and orbit (also attitude for directional instruments) data are merged with the accumulated corrected counts.

(7) Insure that proper documentation and calibration curves are provided to the environment modeling group along with the reduced data within 1 year after launch. This will permit more timely and accurate models to be produced.

(8) Insure that orbital position accuracy is adequate to handle measurements properly where the spatial gradients are large. These regions are at low altitude and in the L range between 2 and 4 where protons exhibit steep radial and energy gradients.

(9) If B/B_o and L coordinates are computed, insure that the same model of the internal field is used and appropriate secular changes are incorporated so that comparisons of measurements from different satellites can be conducted with minimum error.

References

1. Chan, K. W., Sawyer, D. M., and Vette, J. I. (1977) The trapped radiation population, in The Trapped Radiation Handbook, Eds. J. B. Cladis, G. T. Davidson, and L. L. Newkirk DNA 2524 Change 5, Defense Nuclear Agency.

2. Vette, J. I., Ed. (1971) Models of the Trapped Radiation Environment - Volume VII: Long Term Time Variations, NASA SP-3024.

3. Sawyer, D. M., and Vette, J. I. (1976) AP-8 Trapped Proton Environment for Solar Maximum and Solar Minimum, NSSDC/WDC-A-R&S 76-06.

4. Paulikas, G. A., Blake, J. B., and Imamoto, S. S. (1975) ATS-6 Energetic particle radiation measurement of synchronous altitude, IEEE Trans. on Aerospace and Electronic Systems AES-11:1138-1144.

5. Hilberg, R. H., Teague, M. J. and Vette, J. I. (1974) Comparison of the Trapped Electron Models AE-4 and AE-5 with AE-2 and AE-3, NSSDC 74-13.

6. Teague, M. J., and Stassinopoulos, E. G. (1972) A Model of the Starfish Flux in the Inner Radiation Zone, GSFC-X-601-72-487.

7. Teague, M. J., and Vette, J. I. (1972) The Inner Zone Electron Model AE-5, NSSDC 72-10.

8. Teague, M. J., and Vette, J. I. (1971) Variation of the Electron Spectrum in the Inner Radiation Belt, September 1964 to Present, NSSDC 71-11.

9. Singley, G. W., and Vette, J. I. (1972) A Model Environment for Outer Zone Electrons, NSSDC 72-13.

10. Lavine, J. P., and Vette, J. I. (1970) Models of the Trapped Radiation Environment-Volume V: Inner Belt Protons, NASA SP-3024.

11. Lavine, J. P., and Vette, J. I. (1970) Models of the Trapped Radiation Environment-Volume VI: High Energy Protons, NASA SP-3024.

Bibliography

Singley, G. W., and Vette, J. I. (1972) The AE-4 Model of the Outer Radiation Zone Electron Environment, NSSDC 72-06.

Teague, M. J., and Vette, J. I. (1974) A Model of the Trapped Electron Population for Solar Minimum, NSSDC 74-03.

Teague, M. J., Chan, K. W., and Vette, J. I. (1976) AE-6: A Model Environment of Trapped Electrons for Solar Maximum, NSSDC/WDC-A-R&S 76-04.